# The Electro-Optic Beam Position Monitor

By

James DOHERTY, OPEN UNIVERSITY, OXFORD, UNITED KINGDOM

Under the supervision of

Ralph STEINHAGEN, CERN

21st October 2013

**Abstract**

This reports outlines the development of a new ultra-wideband electro-optic beam position monitor (EO-BPM) for use in the Large Hadron Collider (LHC) which utilises birefringent crystals and the Pockels effect to monitor beam position. The physical principles behind the operation of the device and tested topology, which incorporates two Lithium Tantalate crystals, is discussed.

# 1 Introduction

The LHC is the world's highest energy particle accelerator with a circumference of 27 km and is at a depth of between 100 m to 150 m below the Swiss-Franco border. It has collided particles with energies of up to 4 TeV and demonstrated the existence of the HIGGS BOSON. The LHC will continue to address fundamental unsolved mysteries of Physics as its energy levels are increased to 7 TeV in the coming years.

An important performance indicator of circular accelerators is the maximum beam particle intensity that can be injected, accelerated and stored. This intensity is fundamentally limited by self-amplifying beam instabilities, intrinsic to unavoidable imperfections in accelerators. For the highest beam intensities, the beam can no longer be considered as a collection of non-interacting single particles but exhibits, in addition to 'single-particle' effects, more significant 'collective effects' [1].

A notable collective interaction is the 'Head-Tail' instability phenomenon which is caused by a resonance condition in circular accelerators, created by the interplay between beam induced transverse wake fields and longitudinal synchrotron oscillation of the particles within a bunch. The effect has been first observed at the ACO and Adone lepton storage rings in Frascati, and independently been theorised by Sands and Pellegrini [2, 3].

The same phenomenon was later directly observed at CERN's Proton Synchrotron (PS) and Booster (PSB) (both hadron accelerators), and the theory was further formalised by Gareyte and Sacherer [4, 5, 6]. Beside the finite impedances of the beam vacuum chamber that can drive head-tail instabilities, there are a multitude of other effects such as beam-beam interactions, effects related to electron cloud, or other transverse mode coupling instabilities (TMCI) that can drive these 'intra-bunch' motion and that are discussed in detail in [1].

This report discusses the prototype studies related to a novel wide-band beam position monitor pick-up (BPM) based on electro-optical sampling of the transverse intra-bunch motion. The described prototype tests are based and related to earlier studies described in [7, 8, 9].

## 1.1 Intra-bunch beam position detection

Historically, direct observations of intra-bunch motion were made in the time-domain, using wide-band transverse beam position pick-ups connected to an RF hybrid (effectively generating the analog difference between two opposing electrodes) and acquired by fast oscilloscopes [4]. An early PSB measurement example of such a system observing higher-order head-tail motion is shown in Figure 1.

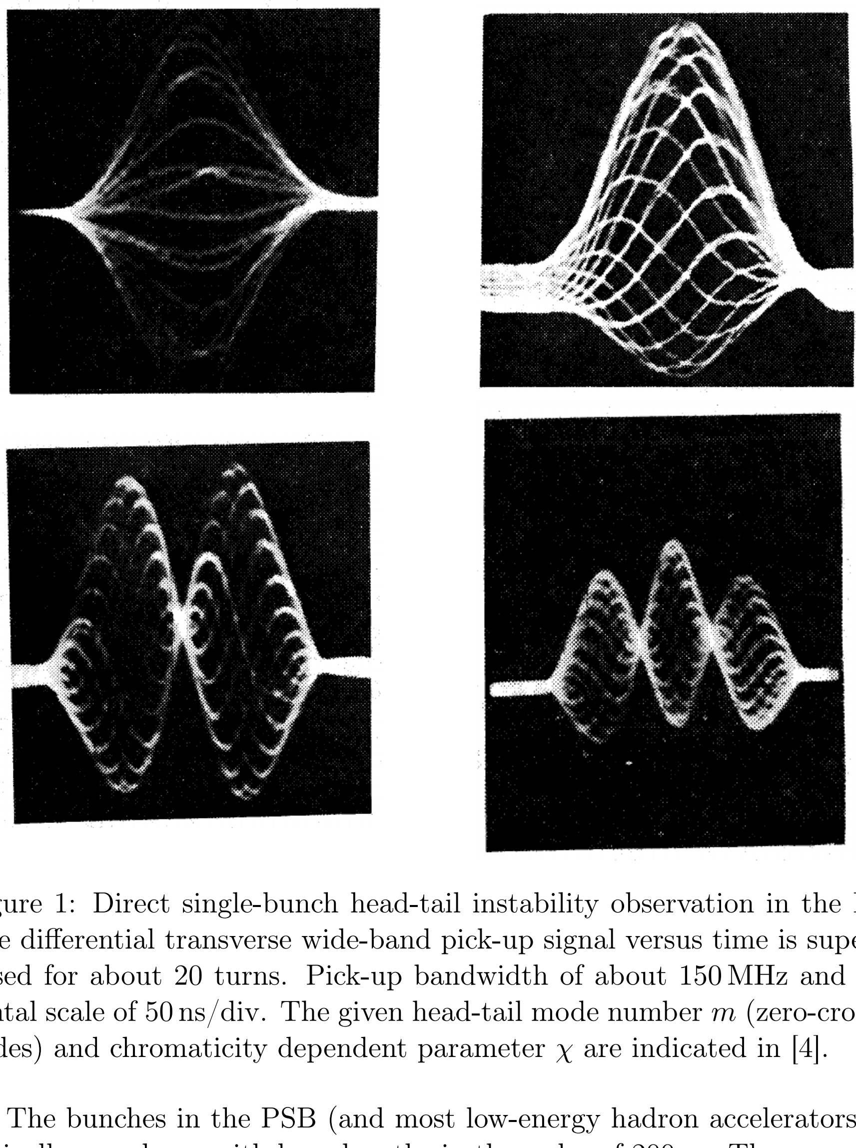

Figure 1: Direct single-bunch head-tail instability observation in the PSB. The differential transverse wide-band pick-up signal versus time is superimposed for about 20 turns. Pick-up bandwidth of about 150 MHz and horizontal scale of 50 ns/div. The given head-tail mode number $m$ (zero-crossing nodes) and chromaticity dependent parameter $\chi$ are indicated in [4].

The bunches in the PSB (and most low-energy hadron accelerators) are typically very long, with base-lengths in the order of 200 ns. Thus an effective analogue RF system (incorporating a pick-up, cabling and oscilloscope) of bandwidth 150 MHz was sufficient to resolve these intra-bunch instabilities. The required minimum system bandwidth increases with decreasing bunch length. Thus the exploitation of the same basic detection principle in high energy and lepton accelerators implies the use of digitizers operating at speeds of 20 GHz or above is required to resolve oscillations in the less than 1 nano-second short particle bunches. However, at these speeds, the effective resolution of even state-of-the-art technology limits the effective intra-bunch position resolution to a few tens of micro-metres. For example, in the LHC, beam particle oscillations at this scale – outside of special machine development studies – cause partial or a total loss of the beam due to the tight constraints imposed on transverse oscillations by the LHC collimation system, which protects LHC's sensitive cryogenic aperture.

## 1.2 Electro-magnetic beam position monitors

To feed a beam of particles through a narrow pipe and around various obstacles, accelerator operators need instrumentation and diagnostics to precisely measure the position of the beam. The importance of this function is two-fold: the beam needs to be well controlled so that it collides accurately with its target, and – especially in high energy machines – to control the available aperture to minimise the spray of high energy particles into the machine which may quench superconducting magnets or potentially damage sensitive equipment.

Electrostatic button and strip-line pick-ups are the most common types of BPMs employed in today's accelerators. These detect the (change-of) image current induced on the vacuum chamber by the charged particles circulating in the accelerator. Electrostatic button BPMs provide a simple way of determining beam position as the induced charge accumulating on the electrodes, and therefore the potential difference across the electrodes, is linearly dependent on the electric field created by the beam. [10]. Strip-line couplers have metallic isolated strips which are parallel to the beam and measure an induced voltage signal to varying degrees depending on their proximity to the charged beam. Figure 2 shows a typical geometry of the source beam charge density and induced signals on the vacuum chamber wall for a button-type or strip-line type BPM.

The amount of obtainable signal depends on the azimuthal coverage and on the electrode length if it is comparable to the bunch length ($2\sigma$). For an off-centre beam, the image charge density on a wall segment at an angle $\theta$ and vacuum chamber radius $R$ can be written as:

$$J_{\text{image}}(r, \phi, R, \theta) = \frac{J_{\text{bunch}}(r, \phi)}{2\pi R} \frac{1 - (\frac{r}{R})^2}{1 + (\frac{r}{R})^2 - 2\frac{r}{R}\cos(\theta - \phi)}$$

And as such the currents flowing through the left and right segment respectively is:

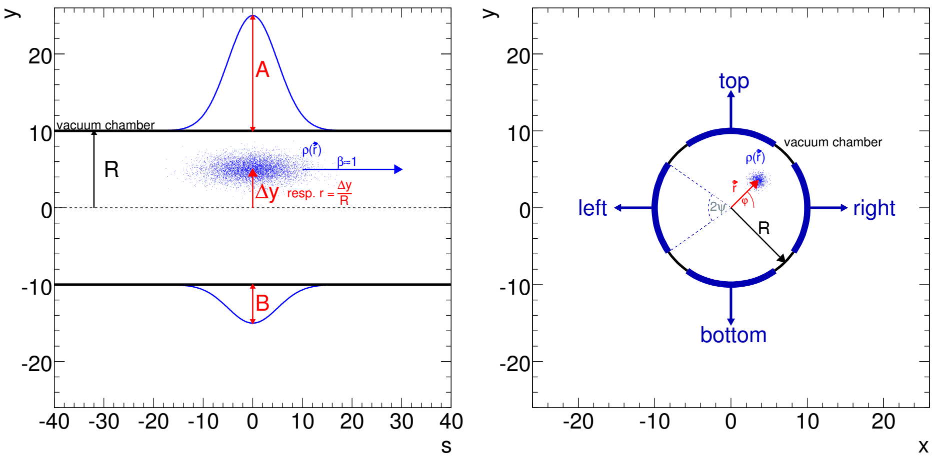


(a) Longitudinal pick-up cross section (b) Transverse pick-up cross section

Figure 2: Button-type BPM principle: The longitudinal (left) and transverse (right) cross section are shown. For relativistic particles the longitudinal bunch structure to first order is projected onto the image charge current on the vacuum chamber. The buttons are isolated from the vacuum chamber.

$$I_L = \frac{I_w}{2\pi}[2\psi + 2\frac{x_0}{R}\sin\psi + \frac{x_0^2 - y_0^2}{R^2}\sin(2\psi) + h.o.]$$

$$I_R = \frac{I_w}{2\pi}[2\psi + 2\frac{x_0}{R}\sin\psi + \frac{x_0^2 - y_0^2}{R^2}\sin(2\psi) + h.o.]$$

The normalised position z is typically written as:

$$z_{\text{norm}} = \frac{\triangle}{\Sigma} = \frac{I_L - I_R}{I_L + I_R}$$

The classic electro-magnetic time-domain based diagnostics systems in most hadron accelerators are fundamentally limited by the available bandwidth of the pick-up and hybrid to about 10 GHz.

## 2 Optics

The EO-BPM uses a pair of crystals, each located at opposite sides of the vacuum chamber, whose birefringence is modified by the electric field of the charged particle beam that passes in between them. The change of birefringence depends on the electric field which itself depends on the beam position, and is measured using polarised laser beams. In order to understand the operation of the proposed EO-BPM, it is useful to summarise a few principles of optics.

Visible light is a transverse electromagnetic wave motion with wavelength ranging between about 390 nm and 740 nm. These waves may be linearly, elliptically or circularly polarised, as illustrated in Figure 3.

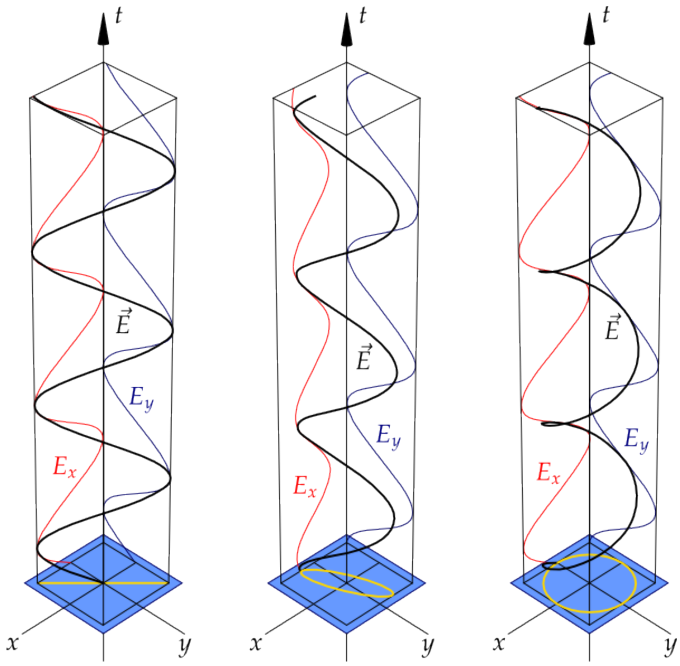


Figure 3: The linear, elliptical and circular polarisation of light. [13]

Birefringence is the resolution or splitting of a light wave into two unequally reflected or transmitted waves by an optically anisotropic medium, as illustrated in Figure 4. A birefringent medium has different refractive indexes depending on the plane of polarisation.

## 2.1 The Pockels effect

Optical birefringence can be induced in a medium by the presence of a constant or varying electric field. One distinguishes the Pockels effect, which is linear, from the Kerr effect, which is quadratic with the applied electric field strength. These effects are represented in the following equation:

$$n(E) = n_o + r_{\mathrm{ij}}E + s_{\mathrm{ij}}E^2$$

with $n(E) =$ being the altered refractive index of the material, $n_0$ the original refractive index of the material, $r_{ij}$ the Pockels coefficient, $s_ij =$ the Kerr coefficient, and $E$ the applied electric field strength, with the sub-indices $ij$

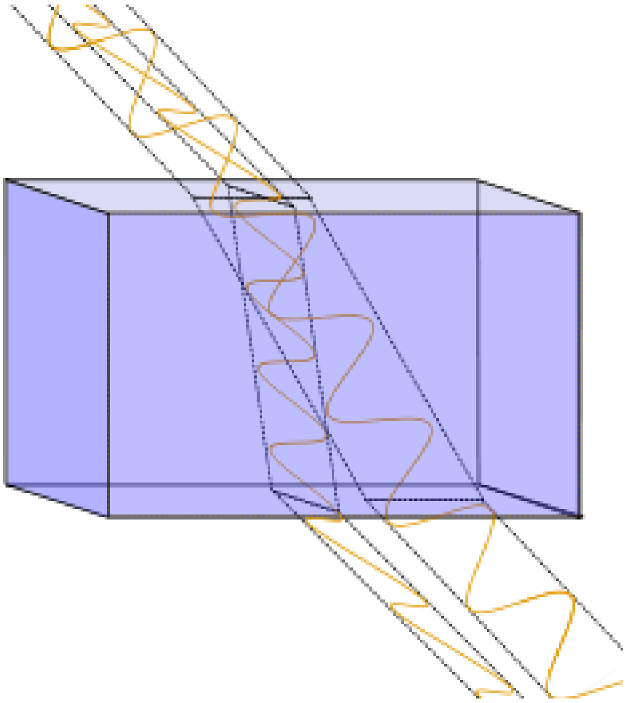

Figure 4: The splitting of light due to being polarised in two planes which have different refractive indexes. [11]

indicating whether the external electric field is being applied parallel to or orthogonal to the electro-magnetic field vectors of the incident light. Other than in anisotropic crystals, for which the Pockels coefficient does not depend on the orientation of the crystal lattice, the crystals are typically cut so that the change of refractive index is parallel to the external electric field. Any electro-magnetic wave can be decomposed into a component that is parallel and another that is orthogonal to the externally applied electric field. Once split, the two waves propagate with different electric field strengths as follows:

$$E_x = E_0 \cos(\omega t - \frac{2\pi}{\lambda} n_x z)$$
$$E_y = E_0 \cos(\omega t - \frac{2\pi}{\lambda} n_y z)$$

One can show that the phase difference between the two wave components is given by

$$\Delta\phi = \frac{2\pi}{\lambda}(n_x - n_y)L = \frac{2\pi}{\lambda}(n_{x_0} - n_{y_0})L + ...$$

and for the longitudinal modulator:

$$\frac{\pi}{\lambda}(r_x n_{x_0}^3 - r_y n_{x_0}^3)V$$

or for the transverse modulator:

$$\frac{\pi}{\lambda}(r_x n_{x0}^3 - r_y n_{x0}^3)\frac{V}{d}L$$

Typically one defines a 'half-wavelength voltage' $V_\pi$ to describe electro-optical modulators, i.e. the voltage required to achieve destructive interference.

$$\Delta\phi = \pi \rightarrow V_\pi = \frac{\lambda}{r_{33}n_e^3 - r_{13}n_0^3} \cdot \frac{d}{L}$$

with $\lambda$ being the wavelength of the incident light, and crystal height $d$ and length $L$ being free parameters of the setup. Notably, $\Delta\phi$ scales with length of the birefringent crystal.

## 2.2 Stress induced birefringence

Stress induced birefringence is the inducement of birefringence in an optical medium by the application of mechanical forces. For example, when an optical fibre is bent, it is compressed in the radial direction of the bend and expanded in the direction perpendicular to it. The refractive index of glass is lowered where it is compressed and raised where it is expanded thus producing a birefringent effect.

## 2.3 Polarisation control

Waveplates are optical devices that alter the polarisation state of light travelling through them. There are two common types of waveplate:

1. Half waveplates ($\frac{\lambda}{2}$ waveplates) which shift the polarisation direction of linearly polarised light; and
2. Quarter waveplates ($\frac{\lambda}{4}$ waveplates) which convert linearly polarised light into circularly polarised light and vice verse.

Fibre-loop retarders, or polarisation controllers, such as that pictured in Figure 5, utilise stressed induced birefringence in optical fibres to create three fractional waveplates that alter polarisation in optical fibres. The fibre is wrapped around three independent spools to create three waveplates and a controlled amount of stress-induced birefringence is used to change the retardance without interrupting the transmission of light in the fibre.

The amount of birefringence induced in the fibre is a function of the fibre cladding diameter, the fixed spool diameter, the number of fibre loops per spool, and the wavelength of the light. The fast axis of the fibre, which is

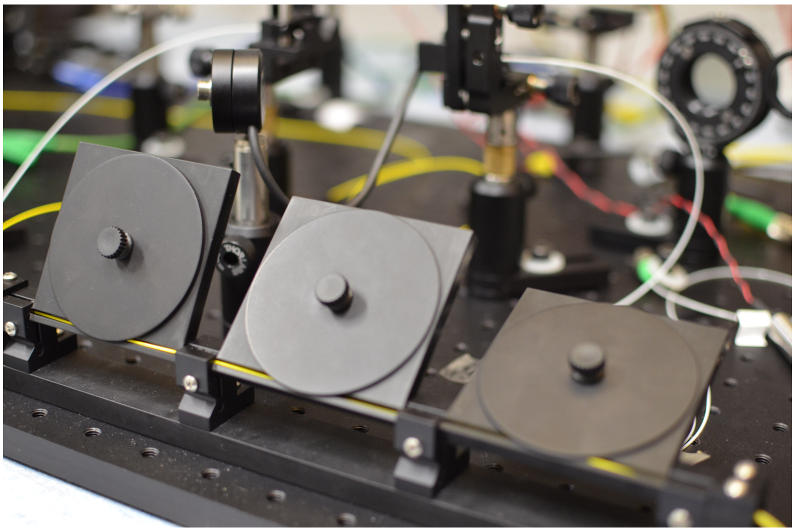

Figure 5: Polarisation controllers - an optical fibre is wrapped around three independently rotating paddles to utilise stress-induced birefringence to control the polarisation of light passing through.

in the plane of the spool, is adjusted with respect to the transmitted polarisation vector by manually rotating the paddles. Ideally, the controller should combine a $\frac{\lambda}{4}$ waveplate, a $\frac{\lambda}{2}$ waveplate, and another $\frac{\lambda}{4}$ plate. When conversion of elliptical to linear polarisation is required, the $\frac{\lambda}{4}$ waveplate is orientated so that the elliptically polarised wave going into the loop is converted into a linearly polarised wave upon exiting the loop. The $\frac{\lambda}{2}$ waveplate may then be used to rotate the polarisation through a given angle. The second $\frac{\lambda}{4}$ waveplate can transform the linear state into an arbitrary polarisation state.

# 3 The electro-optic BPM

## 3.1 Proposed topology

Various topologies have been considered for the EO-BPM, including the Mach-Zehnder and Michelson interferometer topologies as shown in Figure 6. However, initial tests in the laboratory have revealed that these suffer from certain drawbacks:

- there is a need to maintain polarisation within a larger structure;
- they are relatively delicate with respect to alignment, stability of mirrors and split ratio — which would need to be altered close to pick-up for re-tuning;

- the structure size is limited by coherence length, laser line-width and stability, which is manageable in the lab but challenging with respect to in-tunnel operation; and
- they are rather susceptible to temperature stability due to the fairly large size of the interferometer.

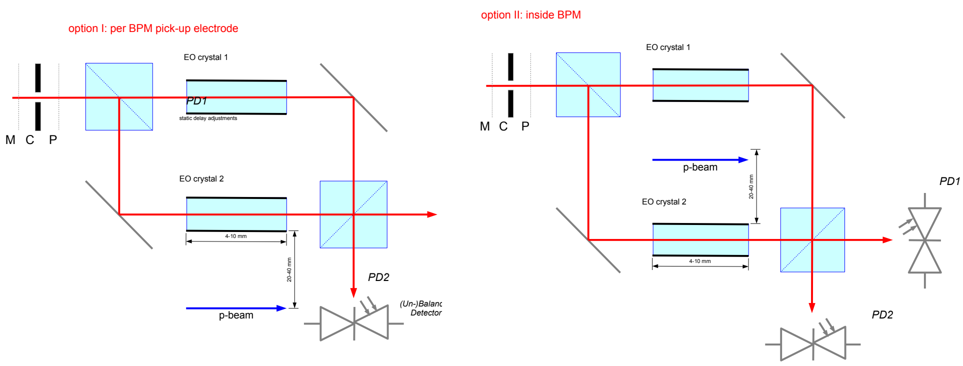


(a) Mach-Zehnder topology. (b) Michelson topology.

Figure 6: Topologies considered for the EO-BPM. [12]

The proposed and further studied EO-BPM's topology is shown in Figure 7, and includes a birefringent crystal located on each side of the beam. Each crystal is flanked by two polarisers, which shall be referred to as the 'polariser', prior to the crystal, and the 'analyser', after the crystal. (N.B. This arrangement is also used in Pockels cells and LCD screens). Light passing through the polariser, analyser and crystals continues to two separate light sensors. The difference in the light intensity striking each of these sensors is converted to an electrical signal [8]. This sum/difference reading will provide information the position of the beam. It is envisaged that the laser beam will be coupled into optical fibres.

The research reported in this paper considers one limb of the proposed topology from laser to light sensor.

## 3.2 Birefringent crystal pick-up

The proposed topology incorporates a Lithium Tantalate ($LiTaO_3$) birefringent crystal. This is similar to Lithium Niobiate ($LiNbO_3$) crystals which are widely used in telecommunications, but offers increased durability. The crystal can be used as the basis for an electro-optical pick-up. When the beam of charged particles in an accelerator changes position relative to the crystal, the strength of the electric field which the crystal experiences changes. This

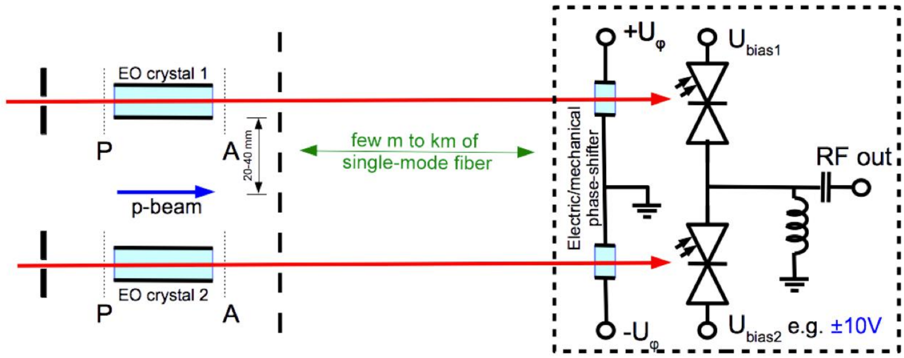


Figure 7: The proposed topology - two crystals, one located on either side of the beam, are flanked by a polariser and analyser. Light from a laser travels through the polarisers, crystals and analysers before striking two light sensors. The difference in reading on the light sensors provides information on the location of the beam. [12]

causes the refractive indexes of the crystal to change which, in turn, alters the degree of rotation of any light passing through the lattice. By using a light sensor to monitor the change of intensity of a laser beam passing through the polariser, crystal and analyser, we can calculate the change in refractive index of the crystal, and thus deduce the position of the beam. This proposed system works in a similar way to the electrostatic and electromagnetic BPMs described above, except that it is the change of refractive index of the crystal, rather than a change in voltage, from which beam position is calculated.

One of the key goals for the electro-optic pick-up is to develop an arrangement whereby, when there is no beam in the machine, the light sensors register zero or very low light intensity. When the beam is in the middle of the accelerator, or its optimal position, the light sensors should register a equal signals. Then, when the beam changes position, the refractive index of the crystal changes and the light passing through each crystal is rotated to a different extent. More light therefore passes through the analyser of the crystal towards which the beam has moved and less light passes through the analyser of the crystal away from which the beam has moved. This series of events is illustrated in Figure 8.

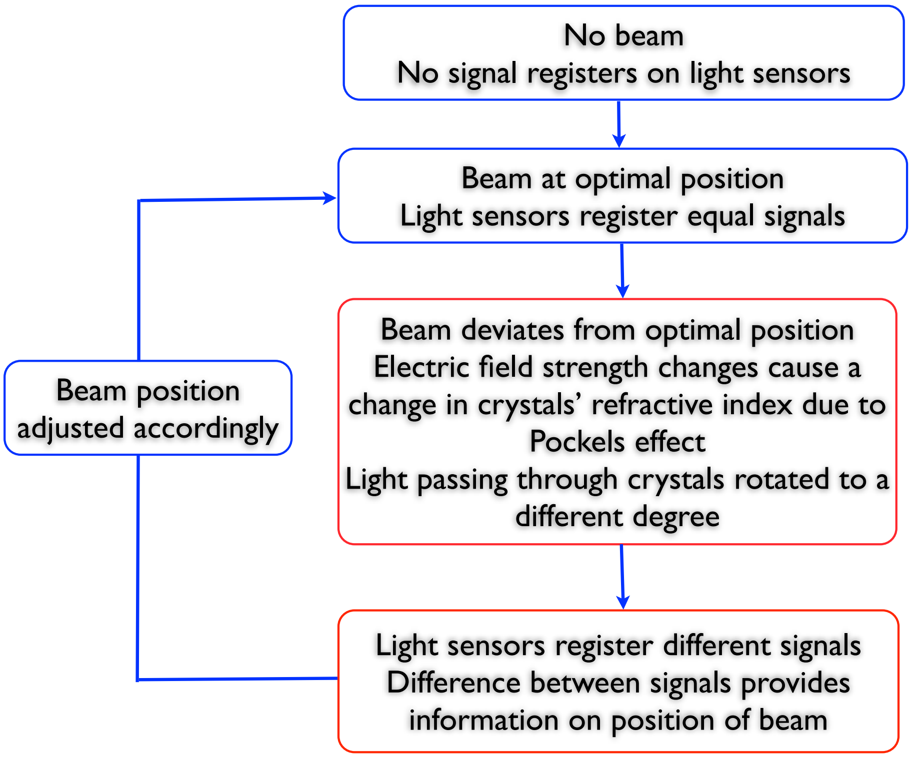


Figure 8: Flow diagram of the operation of EO-BPM.

## 3.3 Advantages

As discussed in the introduction, it is crucial that BPMs with higher bandwidths are developed to monitor intra-bunch head-tail instabilities. An electro-optical set-up offers the possibility of providing a much higher bandwidth pick-up for several reasons.

The crystal is very sensitive to changes in electric field strength, so signal feedback to accelerator operators should be very quick and accurate. The EO-BPM also benefits from the efficiencies of signal transmission through optical fibres. Whereas electric signals through metal cables suffer from relatively severe attenuation, optical signals may be propagated through very long lengths of optical fibre without experiencing anywhere near the same degree of attenuation — which means signals are of much higher bandwidths.

A further advantage of using optical fibres is that, while the polariser, crystal and analyser must be located in close proximity to the beam, the signal can be routed to the remaining hardware and other more complex components that can be located on the surface. The crystal which will be used in the accelerator will be only a few millimetre in length. It is therefore much smaller than equivalent strip-lines at similar bandwidths and it may therefore be possible to place electro-optical BPMs in locations where the current generation of BPMs are too large to fit.

# 4 Aims

The key experimental aims in developing the EO-BPM are as follows:

1. To classify the polarisation of the lasers in use;
2. To verify that $LiTaO_3$ crystals react as predicted by the Pockels effect — this will involve proving that a change in electric field strength alters the refractive index of the crystal and therefore the ellipticity of light passing through it;
3. To test the effect of the crystal on the power and polarisation of light passing through it;
4. To test the sensitivity of the crystal to temperature;
5. To couple the laser beam into the optical fibres, through the crystal, back into an optical fibre and to the light detector;
6. To calibrate a polarisation controller to linearly polarise light entering and leaving the crystal; and
7. To test a mock set-up of one limb of the EO-BPM to check that, in theory, it works.

# 5 Experiments and analysis

## 5.1 Classifying the laser

The experiments performed involved the use of a laser. As the polarisation of light as it enters and leaves a birefringent crystal is critical, it is necessary to measure the polarisation of the light sources used. In the experimental set-up, a green laser and red laser were used. The lasers were secured on a mount and aimed through an iris to ensure a clean focused beam was tested. The beam then passed through a circular film polariser before striking a light sensor. The polariser was rotated about 360° in 10° steps with the corresponding signal level recorded at each step.

Figure 9 and Figure 10 show plots of the angle of the analyser against signal output from the red and green lasers respectively. Figure 10 shows that the green laser is weakly polarised while the red laser has a stronger linear polarisation. Both Figure 9 and Figure 10 show that the green laser is significantly more powerful than the red.

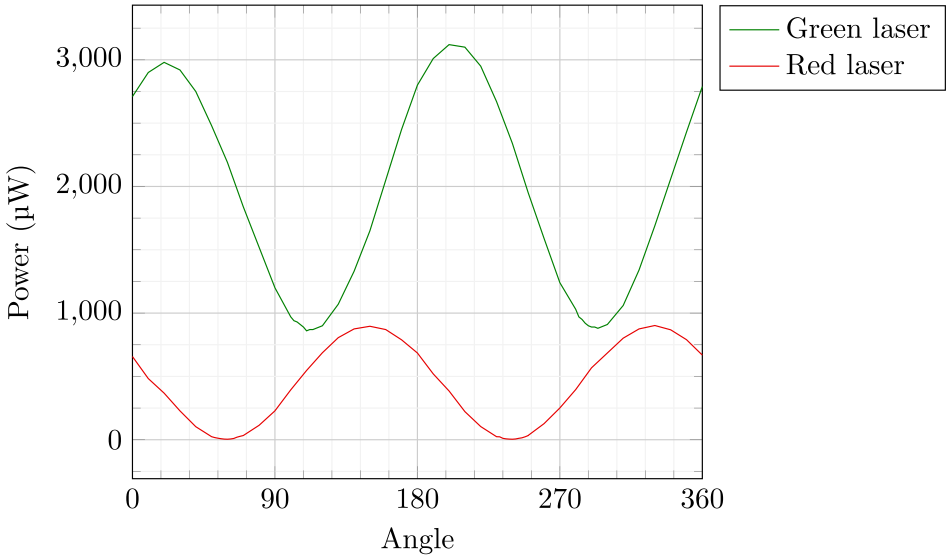


Figure 9: Plot of angle of analyser against signal: the green laser is significantly more powerful than the red.

Despite the red laser being more strongly collimated and polarised, the green laser was significantly more powerful and was therefore used for subsequent experiments. The green laser does however contain a strong infra-red element and so was passed through an infra red (IR) filter. The red laser was used for coupling the green laser into an optical fibre described in subsubsection 5.5.2.

This experiment illustrates the importance of controlling the light both entering and leaving the crystal to ensure the same is linearly polarised.

## 5.2 Effect of crystal on laser

To investigate the effect of the crystal on light propagating through it, the experimental set-up shown in Figure 11 was used. The crystal was removed from the Figure 11 set-up and the polariser set to 45°. (This is because the crystal polarises light in the vertical and horizontal planes so the laser should be split roughly evenly between these planes). The analyser was

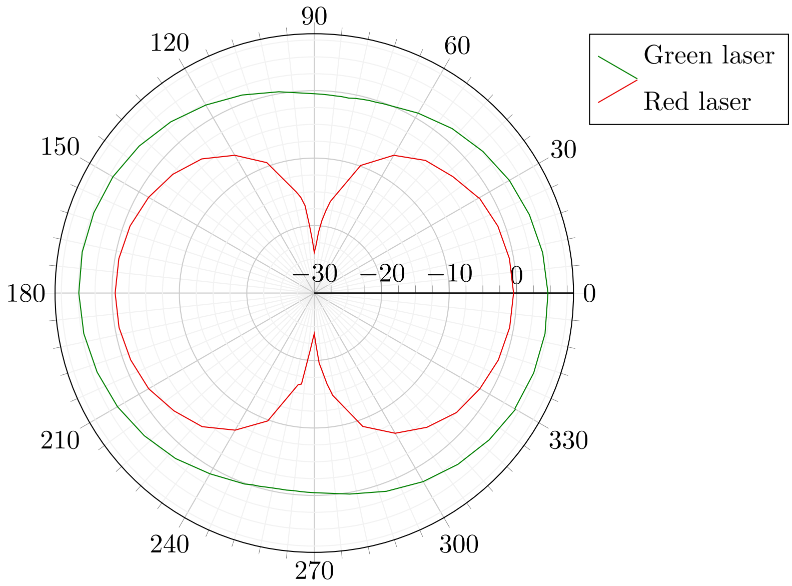


Figure 10: Polar plot of angle of analyser against signal (in dBm): the red laser is more linearly polarised and collimated than the green, but the green is significantly more powerful.(N.B. these plots have been rotated for ease of interpretation.)

rotated through 360° in 10° steps. For each 10° step, the corresponding reading from the light meter was recorded. The crystal was then replaced in the arrangement (with no voltage applied) and the same process repeated.

The data collected with no crystal is displayed as the blue plot in Figure 12 and Figure 13. As expected, the plot in Figure 12 is a good approximation to a sine wave. When the analyser is at 45°, its plane of polarisation is in line with the polariser and the light intensity recorded is at its greatest. There is a further peak at 225°. Conversely, when the analyser is at 135°, the power drops to zero as the polariser and analyser are out of phase and the light is wholly obstructed. This represents an ideal scenario and is how we wish the EO-BPM topology to operate. It will then be possible to arrange the polariser and analyser so that when there is no the beam in the machine, no light reaches the detector.

The red plots in Figure 12 and Figure 13 represent the data collected when the crystal was introduced into the arrangement. The power levels decreased with a maximum signal of just over 400 µW, as compared to over 800 µW without the crystal in place. This loss in signal was expected due to the laser beam being attenuated by internal reflections and other optical effects as it passed through the crystal. The maximum and minimum signals also shifted to the right by approximately 90°, showing that the crystal intro-

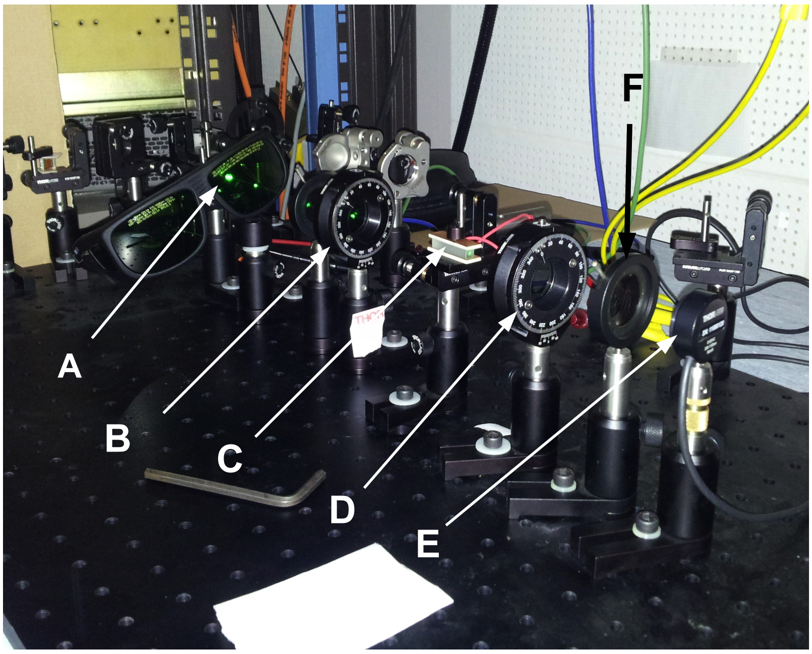


Figure 11: A. The green laser is propagated through an infra-red filter (safety glasses in this instance) B. the polariser C. the crystal attached to a variable AC power supply D. the analyser E. a light sensor and F. two iris' are placed in the arrangement to control beam aperture.

duced a certain amount of ellipticity into the linearly polarised laser beam. This effect is expected as the the Lithium Tantalate crystals are naturally birefringent even without an external electric field. A corollary affect of this ellipticity is that power output no longer reaches zero because the light is not linearly polarised. For our set-up, the analyser will need to compensate for this ellipticity and linearly polarise light exiting the crystal so that a zero value may be achieved when there is no beam.

## 5.3 Temperature

The experimental steps detailed in subsection 5.2 were repeated at 19°, 21°, 23°, 24°, 25° and 31° to test the crystal's response to temperature change. An air-conditioning unit was used to control the ambient temperature. The data is collected presented in Figure 14. Higher temperatures appear to produce lower power outputs while colder temperatures appear to cause higher outputs. However, the highest and lowest temperatures recorded, being 31° and 19° overlap. This suggests that temperature may affect the crystal in a

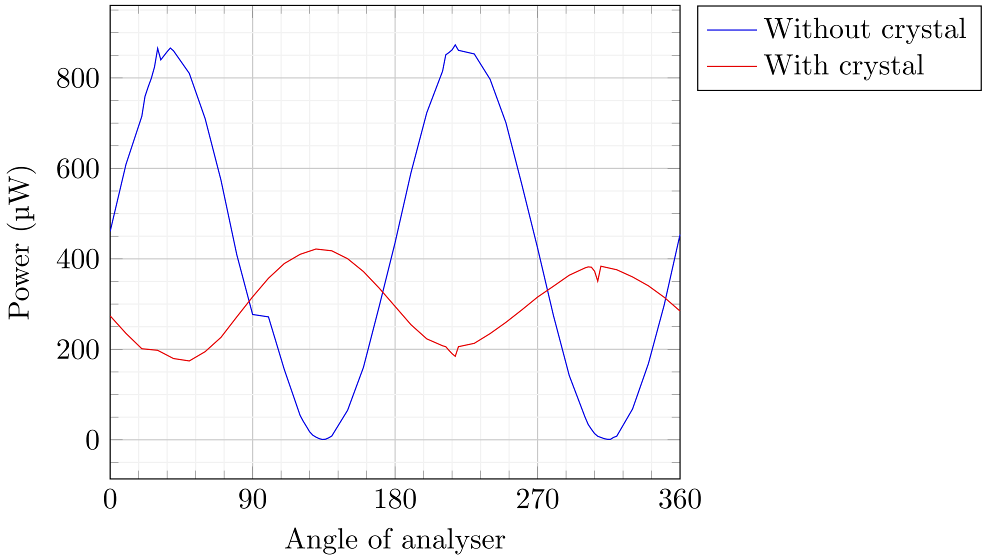


Figure 12: Plot of angle of analyser against light intensity.

modal way.

When the crystal changes temperature it expands or contracts. This means the light passing through the crystal will be in the crystal medium for a longer or shorter period of time, depending on the relative temperature. Therefore, the laser is exposed to the crystal's refractive indexes for longer and so will be less or more elliptical on its exit from the crystal. The thermal expansion of Lithium Tantalate is about $16 \cdot 10^{-6} K^{-1}$ or $4 \cdot 10^{-6} K^{-1}$ depending on the given plane. The length of the crystal actually used in EO-BPM will likely be less than a millimetre in length – more than a factor ten shorter than the crystal used in the experiments. Therefore, the expansion of the crystal would be only approximately 160 nm for 1 ℃ change of temperature. Thus, for there to be a full rotation in the ellipticity of the laser light passing through the crystal there would need to be an approximately 50℃ change in temperature. In the LHC, the temperature should be stabilised to within 1℃, thus the physical environment is very stable.

In addition, the effects of temperature on the crystals are expected to be largely compensated for as the final output from the proposed topography is given by the difference in readings between the two light sensors. As the two crystals are mounted on the same mechanical structure and exposed to the same temperature conditions, they should contract or expand in unison and so any variations in refractive index caused by temperature should be equivalent in each crystal and therefore compensated for in the output difference reading. The effects of temperature should therefore be negligible for the EO-BPM.

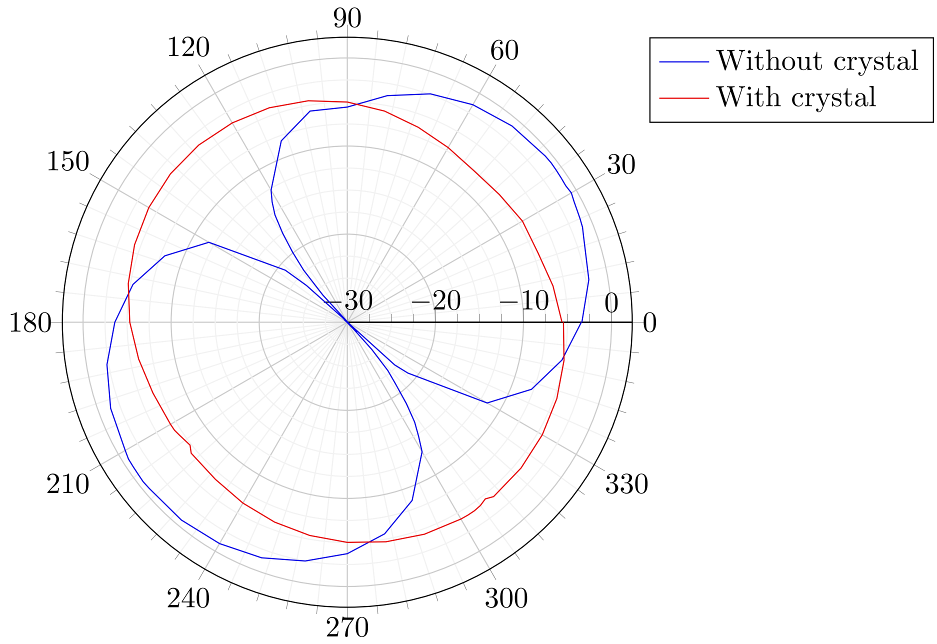


Figure 13: Polar plot of angle of analyser against light intensity.

## 5.4 The Pockels effect

In order to verify that Lithium Tantalate is subject to the Pockels effect, a laser beam was propagated through the crystal then onto a light sensor, as shown in Figure 11. The crystal was attached to an AC power supply and voltages of between 0 and 3 kV were periodically applied while the corresponding readings on the light sensor were recorded against time by an oscilloscope. Data was also recorded on the oscilloscope to probe the modulation and sensitivity of the crystal.

In Figure 15, the red line represents a voltage which was applied across the birefringent crystal. The blue line represents the corresponding light signal recorded. As the voltage across the crystal (being equivalent to the strength of the electric field experienced by the crystal) is varied, the light intensity reaching the photo detector varies between -60 mV and -90 mV. The sections where the blue line is horizontal corresponds to a constant voltage. This data provides confirmation that the Pockel's effect is in operation in the $LiTaO_3$ crystal and that $LiTaO_3$ is, subject to further experimentation, a suitable material to use for in an EO pick-up.

Figure 16 shows the relationship between applied external voltage and observed light intensity. As expected from the Pockels effect, the plot clearly shows a sine wave dependence with the period of twice the half-wave voltage. However, for the purposes of using this for the EO-BPM, only the first fall-

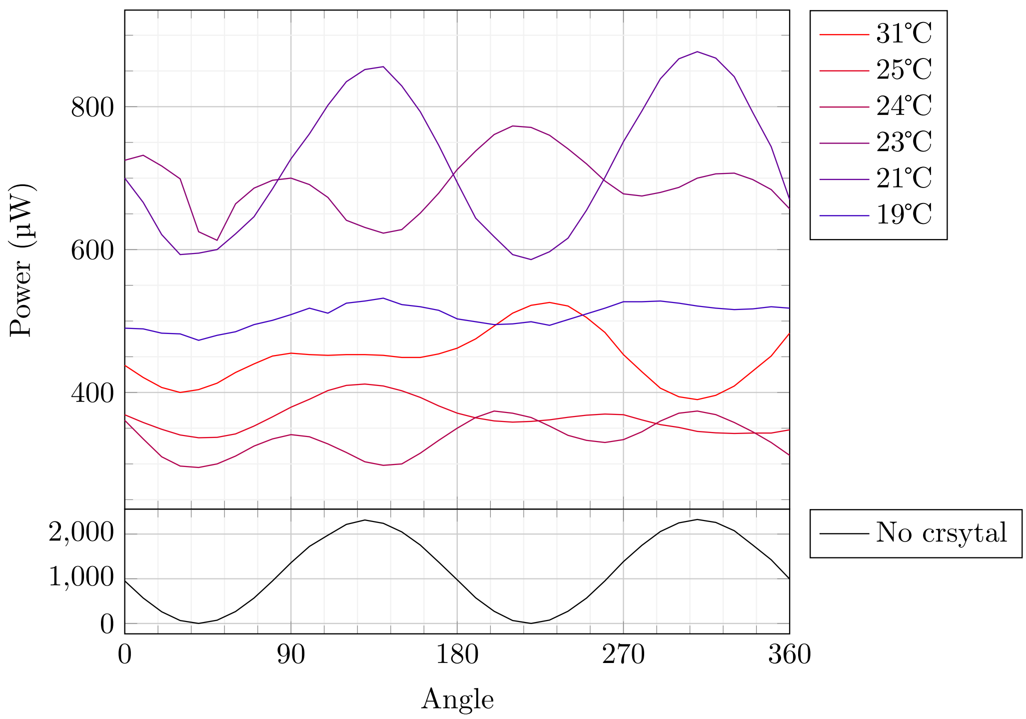


Figure 14: Plot of experiment at various temperatures in air.

ing edge is being used. A half-wave voltage of about 400 V is visible, which defines the maximum useful range for the electric signals that the EO-BPM can handle for the given length of crystal. The crystal length was specifically chosen for the laboratory test for safety and in order to limit the maximum required high-voltage. For the actual deployment in the SPS or LHC accelerator, where peak voltages in the few kV range are expected, the crystal can be kept much shorter. The crystal length needs to be adjusted so that $V_\pi$ is sufficiently large to keep a fairly linear relationship between applied voltage and induced birefringence. The above experiments demonstrate that the set-up and crystal work as required in an 'in-air' setup. The next step was to redo the tests and to couple the set-up into fibres.

## 5.5 Coupling the laser into a fibre

Ultimately, the EO-BPM is to be coupled into optical fibres. Various techniques were tested to find an efficient means of coupling the laser into an optical fibre.

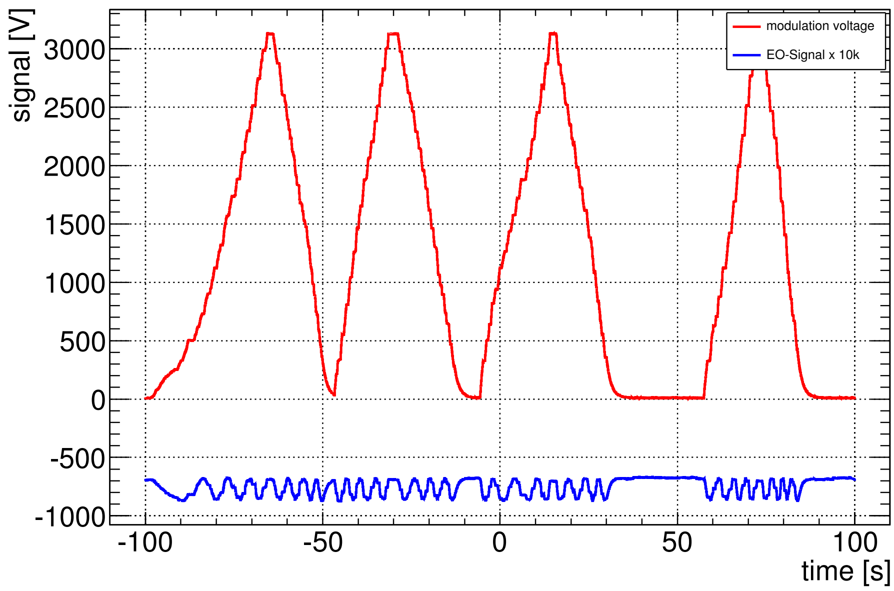


Figure 15: Plot of voltage applied to the crystal against signal — as voltage applied varies, signal varies.

### 5.5.1 Microscope

A specifically designed microscope was mounted on a pedestal and the laser aimed into its lens. A lens attached to an optical fibre was placed next to the other end of the laser so that the magnified laser light entered the microscope. The steps taken in subsection 5.2 and subsection 5.3 were repeated.

The results are shown in Figure 17 and Figure 18, with a dashed black line showing the averaged plots. The data does not exhibit as clean a sinusoidal wave as in Figure 12. The fibre ran through an uncalibrated system of waveplates which will have affected the polarisation of the output light, and perhaps explains why the second maximum peak is lower than the first. Also note that the power output from this arrangement is very low, with a maximum output of under $200\mu W$. At this level, temperature fluctuations and runs in the laser's power can have marked effects on the data collected.

### 5.5.2 Laser-to-fibre coupling

Another more succesful method has been tested, and involves the following steps:

1. The laser, two mirrors and lens attached to an optical fibre were set up in a square arrangement as shown in Figure 19. Each piece of equipment was set at the same height using a ruler.

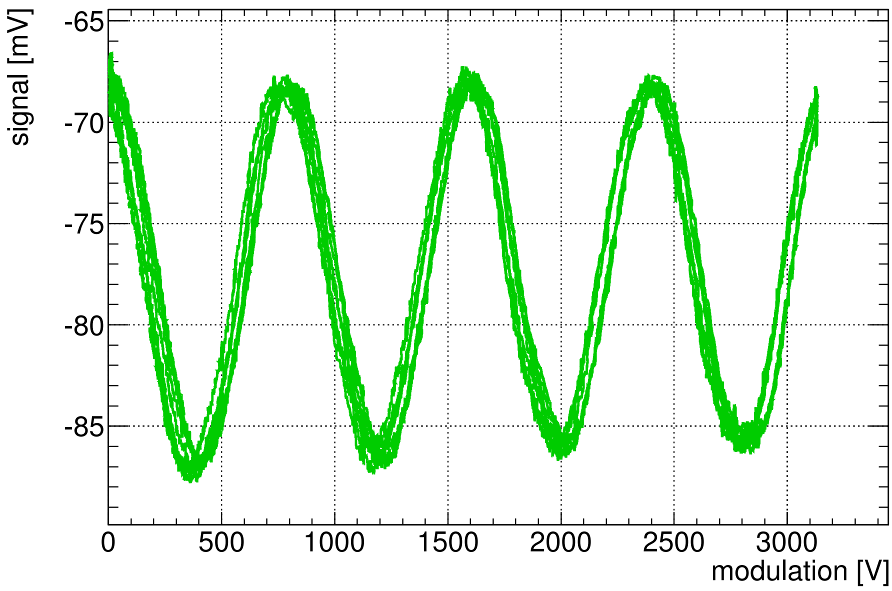


Figure 16: Plot probing the sensitivity of the birefringent crystal — relationship between modulation and signal is linear for our purposes.

2. The laser was turned on and equipment orientated so that the laser beam hit each mirror approximately in the centre before entering the lens. Using a dry ice spray to see the laser beam, each mirror was orientated so that the angle of incidence and reflection of the beam in striking each mirror was 45° i.e. the beam made a 90° angle at each mirror surface.

3. A red laser was coupled into the loose end of the optical fibre using a lens. (This coupling was easy to achieve by had due the more collimated nature of the red laser, however an already fibre-coupled laser could have been used). The red laser emerged at the other end of the optical fibre to provide an alignment beam - a blueprint of the path for the green laser to follow. The position of the apparatus was adjusted so that the red beam roughly struck the centre of each mirror.

4. A piece of white paper was held adjacent to the green laser so that both a green and red dot could be seen. The fine adjustment knobs of the diagonally opposite mirror were adjusted so that the two dots overlapped. The paper was then put over the lens and again adjustments made to the diagonally opposite mirror so that the two dots overlapped. These steps were repeated until the dots overlapped at both the mirror and lens.

5. The red laser was decoupled from the optical fibre and the fibre secured

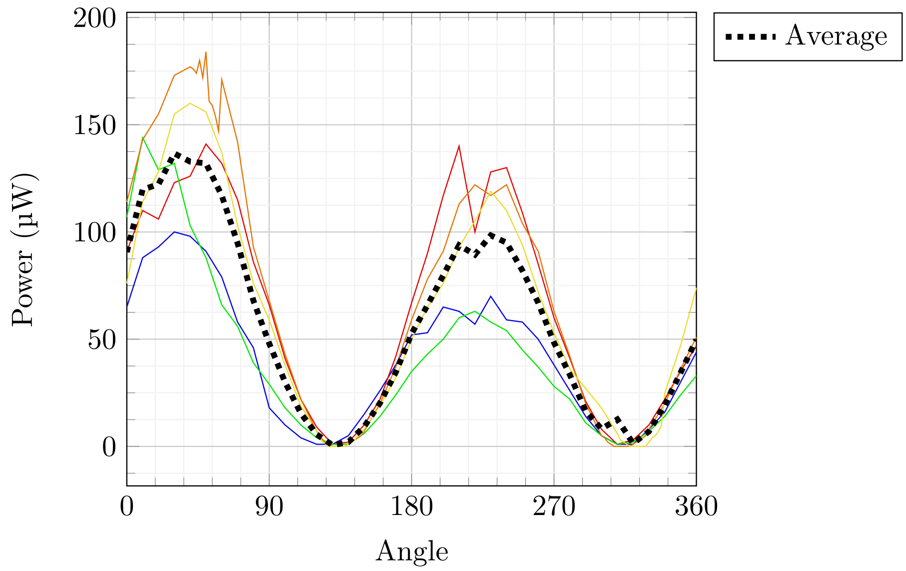


Figure 17: Plot showing angle of analyser against power output in a fibre-coupled set-up.

to a light sensor. There was a sufficient coupling with the green laser to register power on the light sensor.

6. A fine-tuning knob on the mirror opposite the laser was chosen and gently twisted. If the reading on the light sensor went down, then the knob would be twisted in the opposite direction until a maximum reading was reached. This process was then repeated using the other fine-tuning knobs of the mounted mirrors until a maximum signal value was reached. This method is known as 'walking the beam'. To achieve a good coupling one should ideally couple at least 50% of the power of the laser.

This coupling was successfully achieved using the technique detailed above with approximately 75% efficiency. It therefore represents a much stronger coupling than was achieved with the microscope. It is envisaged that this technique could be used for coupling the laser into the first optical fibre of the EO-BPM.

### 5.5.3 GRIN lens

A gradient-index, or GRIN, lens is designed to couple laser light into optical fibres by 'funnelling' the light into the fibre. The following steps were taken:

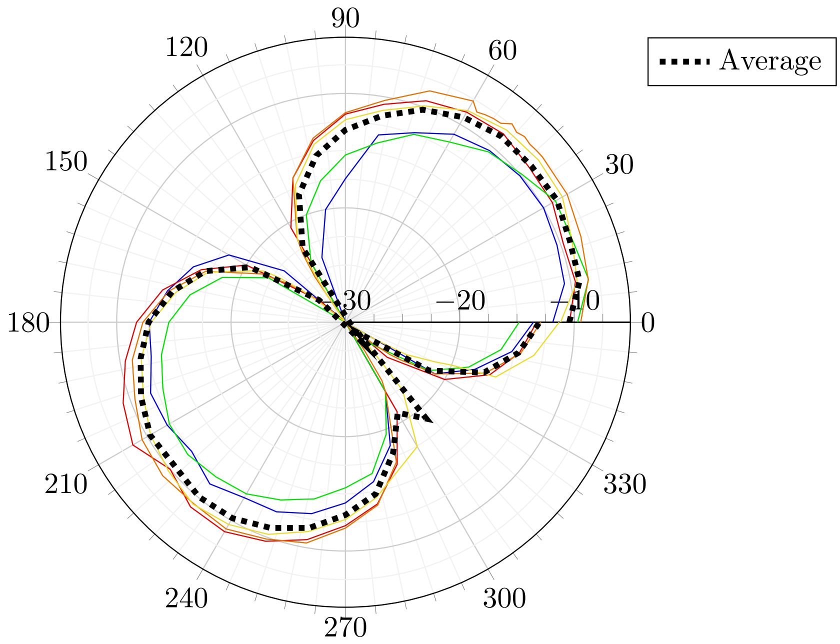


Figure 18: Polar plot illustrating polarisation of the laser in a fibre-coupled set-up.

1. The GRIN lens and a ferrule were secured into a small glass sleeve and attached to the end of an optical fibre into which the green laser was coupled. The lens was mounted on a pedestal which allows fine control positional adjustments. A second GRIN lens, with its fibre being attached to the light sensor, was also mounted on a finely controllable pedestal; and

2. The GRIN lenses were aimed at each other and, using the fine controls to maximise power, the maximum value of signal detected was recorded.

Using this technique, where laser light was already coupled into a fibre using the alignment beam, it was only possible to achieve 2–3% efficiency. Further experimentation using greater degrees of freedom of movement of the GRIN lenses will be required to ensure higher power levels are achieved.

## 5.6 Polarisation

As discussed above, it is necessary to control polarisation of light entering and leaving the crystal. In order to do so, a polarisation controller has been investigated. By wrapping the optical fibre around each spool a certain

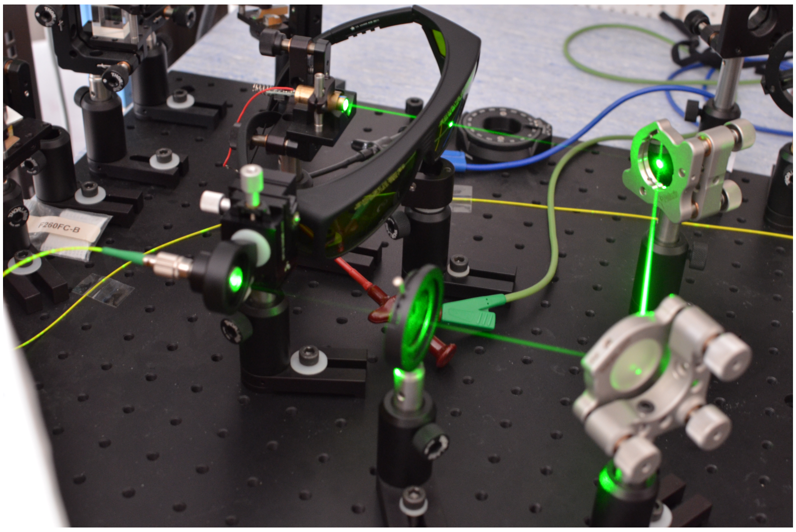

Figure 19: The laser beam, reflecting off two mirrors before entering a lens.

number of times it is possible to create a $\frac{\lambda}{2}$ and $\frac{\lambda}{4}$ waveplates. To calculate the number of loops required, and using a graph provided by the manufacturer of the polarisation controller, a reading was taken for the value of retardance of the 125 µm mono-fibre being used when light of wavelength 532 nm (being the wavelength of our laser) passes through it. The reading was 4.1 rad which corresponds to approximately 234°. This is therefore a retardation of 78° per loop.

The retardance in degrees, the delay per loop for number of loops $1-8$, and the delay per loop modulo 360 were then calculated and are displayed in Table 1. Those delays per loop modulo 360 close to 90° represented the number of loops for a $\frac{\lambda}{2}$ waveplate and those close to 180° were the number of loops required for $\frac{\lambda}{4}$ waveplate. As can be seen from Table 1, 6 and 8 loops are the closest approximations to $\frac{\lambda}{4}$ waveplates with 8 loops having an error of 6° and 6 loops with an error of 18°. 7 loops provides a good approximation to a $\frac{\lambda}{2}$ waveplate with an error of only 6°.

The number of loops were then tested using the polarisation controller using the set-up shown in Figure 20. To do so the paddle was put in a position where the light detector registered its lowest value. The analyser was then adjusted so the lowest value was reached. This was recorded and the process repeated to check the highest values obtainable. If the light exiting the fibre is linearly polarised then the extinction rate should be high and the lowest value of signal approaching zero. If the polarisation is circular then the signal reading should be constant.

On testing the polarisation controller it was possible to create circularly polarised light but not perfect linearly polarised light as required. Although

| No of loops ($i$) | $i$ x $\Delta loop$ (deg) | $i$ x $\Delta loop$ mod 360° (deg) |
|---|---|---|
| 1 | 78 | 0 |
| 2 | 156 | 0 |
| 3 | 234 | 0 |
| 4 | 312 | 0 |
| 5 | 390 | 30 |
| 6 | 468 | 108 |
| 7 | 546 | 186 |
| 8 | 624 | 264 |

Table 1: Table illustrating the numbers of loops of optical fibre to make a $\frac{\lambda}{2}$ waveplate and a $\frac{\lambda}{4}$ waveplate.

the polarisation could be used to provide a certain amount of extinction — this was not absolute. This would tend to agree with our calculations in the table above which show that we do not have perfect waveplates. Thus, this specific type of polarisation controller does not quite provide the sufficiently high levels of polarisation control which we require. It may therefore be necessary to consider fine-tuning the polarisation controller or to use another device for this purpose.

### 5.7 All-fibre EO-BPM test set-up

Once the above steps were taken, it was possible to test a set-up which roughly resembled one half of the proposed EO-BPM topography, as shown in figure Figure 20.

The AC supply and a light sensor were attached to the oscilloscope and varying voltages applied to the crystal. The oscilloscope recorded voltages and corresponding light signals over time. The data displayed in Figure 21 was collected. This plot is similar to that observed at Figure 16 for the in-air set-up. Thus, it is possible to conclude that EO-BPM will, subject to further experimentation and adjustment, function if well coupled into optical fibres.

## 6 Conclusion

This paper has documented the initial steps taken in the development of an EO-BPM. Various topologies for the EO-BPM were considered, but a dual crystal, polariser/analyser arrangement was deemed the most appropriate.

Initial experiments have confirmed that $LiTaO_3$ crystals are birefringent and react to changes in electrical field strength as predicted by the Pockels effect. The crystals are sensitive to changes in temperature but due to the

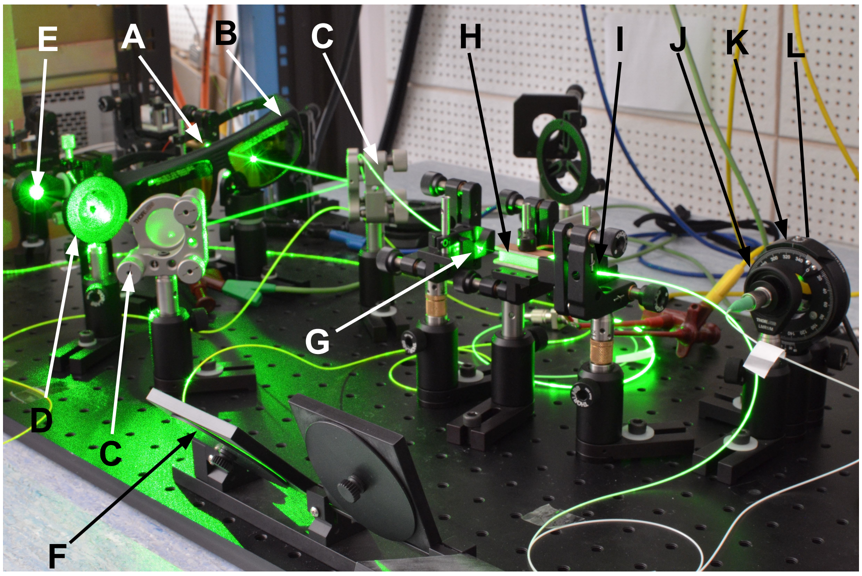


Figure 20: A mock EO-BPM - A. the laser B. an IR polariser C. two mirrors provide six degrees of freedom to control the laser beam D. iris ensures the laser beam is well focused E. using a lens the laser is coupled into the optical fibre F. the three paddles of the polariser controller controls the polarisation of the laser light G. the polarised light emerges from a GRIN lens H. the laser travels through the birefringent crystal I. then re-couples into an optical fibre via a second GRIN lens J. it exits the optical fibre via a lens K. and passes through an analyser L. before finally hitting a light sensor.

small size of the crystals which would be used in the EO-BPM, the controlled environment in which they would be situated, and the use of dual crystals — temperature change should not pose a major issue in the operation of the EO-BPM.

It is envisaged that the EO-BPM will be fibre-coupled. A successful coupling of a laser beam into a single-mode optical fibre was achieved using an alignment beam. A coupling was also achieved between two GRIN lenses but some further fine-tuning will be required to reach higher power transmission. Using multi-mode fibres shall, no doubt, improve efficiency.

A three-paddle polarisation controller was tested. Although the controller produced circularly and elliptically polarised light, it did not provide total control of laser beam polarisation. It is hoped that, with further experimentation, the device will be able to provide linearly polarised light. If not, there are other stress-induced birefringence based polarisation controllers on the market which may offer greater control.

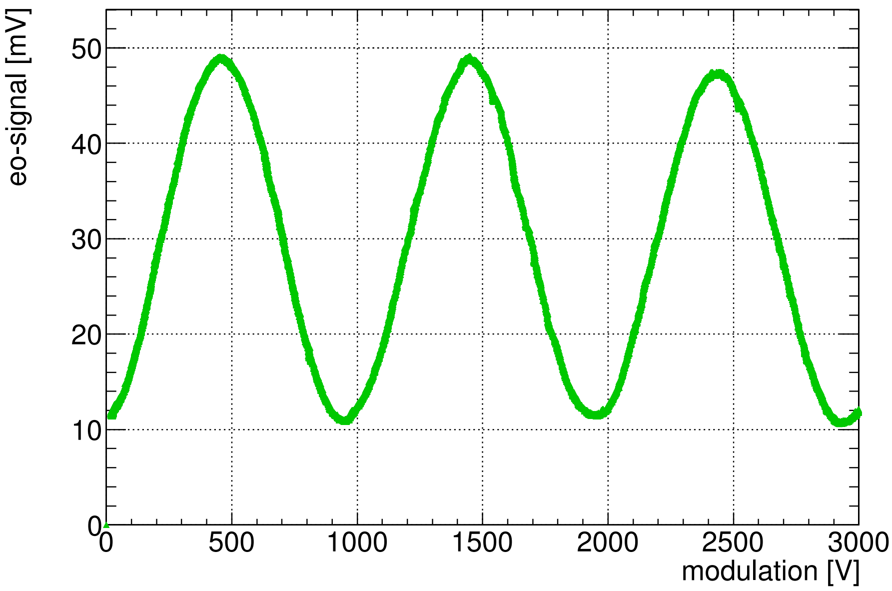


Figure 21: Data collected from the mock EO-BPM set-up. There is a sinusoidal relationship between the voltage across the crystal and the EO signal.

A mock-up of one limb of the EO-BPM was tested and provided satisfactory results and evidence that the principles behind the EO-BPM work. Further refinement of the device will be required before a prototype is built for testing in CERN's Super Proton Synchrotron. It is hoped this happen in 2015.

# 7 Acknowledgements

I would like to thank:

**Ralph Steinhagen** for his excellent supervision on the experimental and theoretical aspects of this research, and for his input on and editing of this report;

**Thibaut Lefevre** for his advice on the practical aspects of the EO-BPM;

**Mark Boland** for his valuable input into the presentation of this work; and

**Joshua Ellis** for his assistance with all things software related.

# References

[1] Stephen Myers ed. and Herwig Schopper ed., "Elementary Particles - Accelerators and Colliders – Chapter 4", Landolt-Bornstein: Numerical Data and Functional Relationships in Science and Technology - New Series / Elementary Particles, Nuclei and Atoms, Vol. 21, Springer, London, ISBN-9783642230523, 2013

[2] M. Sands, "The Head-Tail Effect: An Instability Mechanism in Storage Rings", SLAC-TN-69-008 & SLAC-TN-69-010, SLAC, 1969,

[3] C. Pellegrini, "On a New Instability in Electron-Positron Storage Rings (The Head-Tail Effect)", Nuovo Cim. A64 (1969) 447-473

[4] J. Gareyte, "Head-Tail Type Instabilities in the PS and Booster", CERN-MPS-BR-74-7, CERN, 1974

[5] F. J. Sacherer, "Transverse Bunched Beam Instabilities - Theory", CERN-MPS-INT-BR-74-8, CERN, 1974,

[6] F. J. Sacherer, "Transverse Bunched Beam Instabilities", CERN/PS/BR 76-21, CERN, 1976,

[7] S. Dawson, D.J. Peake, R.P. Rassool, M.J. Boland, R.J. Steinhagen, "Storage Ring Tune Measurements using High-speed Metal-semiconductor-metal Photodetector", IBIC'12, Tsukuba, Japan, 2012

[8] R. J. Steinhagen, M.J. Boland, and T. G. Lucas, R.P. Rassool, T.M. Mitsuhashi, "Application of Metal-Semiconductor-Metal (MSM) Photodetectors for Transverse and Longitudinal Intra-Bunch Beam Diagnostics", IBIC'13, Oxford, UK, 2013

[9] R. J. Steinhagen, M.J. Boland, and T. G. Lucas, "A Multiband-Instability-Monitor for High-Frequency Intra-Bunch Beam Diagnostics", IBIC'13, Oxford, UK, 2013

[10] G. Vismara, "Signals processing for Beam Position Monitors", 2000

[11] M. Haggstrom, Wikipedia, non-copyrighted image

[12] R Steinhagen, "Fast Inter/Intra-Bunch Activities related to CLIC and LHC slides", internal presentation, 1 January 2012

[13] Wikipedia, non-copyrighted image